Peer reviewed version

License (if available):
CC BY-NC-ND

Link to published version (if available):
10.1017/S1431927621000192

Link to publication record in Explore Bristol Research
PDF-document

University of Bristol - Explore Bristol Research
General rights

Low Voltage Electron Probe Microanalysis

of Uranium

Mike B. Matthews[1,2], Stuart L. Kearns[2] and Ben Buse[2]

[1]AWE, Aldermaston, Reading, RG7 4PR, UK

[2]University of Bristol, School of Earth Sciences, Wills Memorial Building, Queens Road, Clifton, BS8 1RJ, UK

Abstract

Electron probe microanalysis of uranium and uranium alloys poses several problems, such as rapid oxidation, large poorly constrained correction factors, and a large number of characteristic x-ray lines.

We show that U metal can grow 10 nm of oxide within ~20 s of air exposure, increasing to 15 – 20 nm within a few minutes, which can produce a 30% quantification error at 5 kV. A 15 nm carbon coating on the UO_2 reference material also produces ~30% quantification error of the uncoated but surface oxidised U sample at 5 kV. Correcting for both the coating and oxide improved the analysis accuracy to better than ±1% down to 7 kV and ~ 2% at 5 kV but the error increases strongly below this.

Measurement of C in U identified a previously unreported U N_6-O_4 line interference on the C $K\alpha$ peak which can produce over 1% error in the analysis total.

Oxide stoichiometry was demonstrated to have only a small impact on quantification. Measurement of the O Kα and U Mα mass absorption coefficients in U as 9528 cm^2/g and 798 cm^2/g respectively show good agreement with recently published values and also produce small differences in quantification error.

1   Introduction

Electron Probe Microanalysis (EPMA) has been an invaluable tool for the nuclear industry since its very earliest days. The first EPMA spectra acquired on Pu were reported in 1961 (Scott, 1961) and within a few years the technique was being used to measure Fe, C and Ga contents in Pu (Scott & Ranzetta, 1961; Ranzetta & Scott, 1964; Hakkila et al., 1964), for the analysis of U-alloys (Colby, 1963, 1966), and for inclusions in UO_2 (Jeffery, 1967). The ability of EPMA to provide non-destructive analysis of almost the entire periodic table down to trace level (less than ~100 ppm) detection limits at micron-scale resolutions (Reed, 1975) is particularly valuable to an industry where the materials are often only available in small quantities, are difficult to handle and prepare and where excess waste is extremely costly.

At 'conventional' analysis voltages (15 - 25 kV) the analysis volume is predominantly a function of the accelerating voltage and the sample's mean atomic number, Z. As the voltage is reduced the volume reduces, increasing spatial resolution, but the diameter of the electron beam becomes an increasingly limiting factor (McSwiggen, 2014). Field emission gun (FEG) electron source EPMA instruments provide 2 – 3 orders of magnitude smaller beam diameters than conventional W-source instruments, making higher spatial resolutions available at low accelerating voltages (<15 kV) (McSwiggen et al., 2011). The commercial availability of FEG-EPMA instruments since 2000 is fuelling a more widespread use of low voltage analyses

but, to date, there has been no systematic investigation of the accuracy of U and U-alloy analysis under these conditions.

U metal and U alloys pose several problems for microanalysis: U oxidises extremely readily, growing a surface oxide film of several nm almost instantly on contact with air (Bowles, 1978; Ranzetta & Scott, 1964; Younes et al., 2007); being a high Z element U emits a large number of x-ray lines (for example, Bearden (1967) lists 80 lines for U), increasing the potential for overlaps when analysed in the presence of other elements (Jeffery, 1967; Ranzetta & Scott, 1964; Walker, 1999); and absorption corrections are large and not well constrained. These problems are exacerbated when analysing at lower accelerating voltages in order to investigate smaller and smaller features, since the energies of x-ray lines that can be excited is decreased, forcing the use of lower energy x-ray lines for analysis. For example, for U this means using the M-lines, for which the correction factors are larger and even less well characterised than for the L-lines (Romig Jr., 1984; Ranzetta & Scott, 1964; Bowles, 1978).

Surface oxides, which may have no detrimental impact on sample quantification at 'conventional' analysis voltages (15 – 25 kV) become increasingly significant components of the analysis volume as the accelerating voltage is decreased. Kitamura et al (Kitamura et al., 1982) were able to analyse U uptake from seawater by absorbent materials using U-metal wire as a reference material for analyses carried out at 25 kV without having to correct for any surface oxide on the wire, but Ranzetta and Scott (Ranzetta & Scott, 1964) found increasingly inaccurate C measurements in UC with decreasing voltage and attributed this to a combination of the surface oxide and large absorption corrections.

Absorption is commonly a significant correction factor in quantification, in particular for very soft x-rays where it can dominate the total correction, making them sensitive to errors in the mass absorption coefficients (MACs) which are used to calculate the degree of absorption of a given element x-ray line by a given absorbing element. Unfortunately, MAC values are generally not well constrained for energies below ~1 keV, leading to large potential quantification errors: An assessment of the Heinrich (1986) MAC values, which form the basis for most currently used tables, reported errors of ~5% for energies above 1 keV but ranging from 10 – 200% below 1 keV (Merlet, 1998).

The Heinrich (1986) values are semi-empirical, being based on an empirical function (Equation 1) between absorption edges, fitted to experimental datapoints compiled by Saloman et al (1988):

$$\mu/\rho = \frac{cZ^4}{A} E^{-n} \left(1 - e^{\left(\frac{b-E}{a}\right)}\right)$$

Equation 1

where μ/ρ is the mass absorption coefficient, μ, per unit density, ρ,

        Z is the atomic number,

        A is the Avogadro Number,

        E is the energy of the absorbed photon,

        a, b and c are parameters derived from fits to experimental MACs, and

        n is an exponent between 2.5 and 3 which varies slowly with Z.

For low energy x-rays, which Heinrich defines as having an energy below the highest N-edge of the absorber material, he proposes a modified version of Equation 1 to achieve a fit to the experimental values:

$$\mu/\rho = 1.02\frac{cZ^4}{A}E^{-n}\left(\frac{E-E_c}{E_n-E_c}\right)$$

Equation 2

where E_c is the lower cut-off value for the extrapolation, and

E_n is the energy of the highest N-line of the absorber.

Farthing and Walker (1990) extended Heinrich's tables to include the actinide elements, using line energies from Kleykamp (1981). For the low energy x-rays they changed Heinrich's adjustment factor in Equation 2 from 1.02 to 0.727 to better fit the values from Henke et al (1982). This earlier semi-empirical compilation focussed on extending and improving the lower energy coefficient values.

Pöml and Llovet (2020) explicitly addressed the absorption of O Kα by the actinide elements Th, U, Np and Pu. They calculated MAC values from EPMA measurements on dioxides of each actinide element using a 'P&P' MAC calculation method proposed by Pouchou and Pichoir (1988). In this study we apply the P&P method to measure O Kα and U Mα absorptions in UO_2 and, from these, calculate the O Kα and U Mα in U MAC values.

Reference materials (RM) for metallic U alloys are also problematic: U-bearing glasses have low U content, requiring large quantification corrections; U metal and high U-alloys oxidise very rapidly in air making analysis of oxide-free surfaces difficult; fully dense, porosity-free 'bulk' UO_2 samples are not readily available; most oxides are electrically insulating so require conductive coating. We test for surface charging of a fully dense synthetic UO_2 using energy dispersive spectra (EDS) acquired on both coated and uncoated UO_2 and compared against materials known to be good electrical conductors. Comparison is made between calibrations using the

UO$_2$ RM uncoated and with a C coating. The magnitude of correction required to correct for this coating is assessed.

The key aim of this study is to quantify the accuracy to which U can be analysed and to investigate the relative impacts of the factors described above. To minimise the number of variables as far as possible, the test sample in this study is reduced to the simplest geometry, an uncoated high purity depleted uranium metal tile. Lacking access to an inert sample preparation and transfer system the tile surface is oxidised. Using thin film analysis tools developed in previous publications (Matthews et al., 2018a, 2019) we investigate the accuracy to which the 100% U composition can be recovered through the surface oxide over a range of accelerating voltages, 5 – 25 kV. We assess the effect on quantification of the substrate of non-stoichiometry of the assumed UO$_2$ surface oxide and also compare quantifications using the P&P method measured O Kα and U Mα in U MAC values against database values.

2 Materials and Methods

2.1 Software

GMRFilm (Waldo, 1988) and the 2014 PENEPMA (Llovet & Salvat, 2016) variant of the PENELOPE (Salvat, 2015) Monte Carlo protocol were used to determine coating and oxide thicknesses from EPMA measured k-ratios using the linear modelling methods described in previous publications (Matthews et al., 2018a, 2019, 2018b). Layer densities of 2.0 g/cm^3 for C and 10.97 g/cm^3 were assumed for all modelling.

Duane-Hunt cut-off values, which are used to quantify the primary beam landing energy on the sample, were measured from acquired EDS spectra imported into the DTSA-II (Ritchie, 2009) Monte Carlo program.

Casino v4.12 (Drouin et al., 2007) was used to calculated theoretical intensity values for Pouchou and Pichoir (1988) MAC calculation method. The P&P method inverts a normal quantification procedure so that instead of calculating an unknown composition using known MAC values, measurements on a known composition are used to determine the MACs as unknowns. Initial MAC values are assigned, and a theoretical composition and x-ray intensities are calculated and compared against experimental measurements over a range of accelerating voltages. The MAC values are then iteratively adjusted until the difference between the theoretical and experimental intensity values summed over all the voltages is minimised.

The default settings, summarised in Table 1, were used for all software packages.

GMRFilm	• Version: 05/1993 • Iterations: max. 15 • $\phi(\rho z)$: Pouchou and Pichoir PAP (1990) (Pouchou & Pichoir, 1990) • mac's: Heinrich IXCOM-11 • Fluorescence: Yes
DTSA-II	• Version: Iona (08/2015) • $\phi(\rho z)$: Pouchou and Pichoir XPP • mac's: Heinrich IXCOM-11 • Ionisation cross-sections: Bote/Salvat 2008 • Probe dose: 600nAs • Fluorescence: Yes

PENEPMA*	- Version: 2014 - Trajectories: 1×10^7 - Fluorescence: Yes S_{max} (film): 1/10th coating thickness - Variance reduction: Yes - Forcing: Yes - Splitting: No
Casino	- Version: 2.5.1.0 - Total and partial cross-sections: Mott by interpolation - Effective ionisation sections: Casnati - Ionisation potentials: Joy and Luo (Joy & Luo, 1989) - Energy loss calculation: Joy and Luo (Joy & Luo, 1989) - Fluorescence: No

Table 1   Default software settings used. See the individual software manuals for descriptions of the parameters.

2.2   Experimental

A 99.99% pure depleted uranium tile of ~10 x 10 mm, fixed with conductive carbon adhesive pads and Ag-paste onto a 25 mm diameter brass block was hand polished flat using diamond suspensions down to 1 μm prior to each analysis session. All other samples and RMs were mounted in 25 mm diameter conductive phenolic resin blocks and ground and polished to 1 μm diamond. Immediately prior to each analysis

session the RMs were cleaned using a 0.05 μm Al_2O_3 oil-based suspension to remove any surface oxides or contaminants and cleaned using isopropanol then ethanol to ensure oil and residue-free surfaces (Pinard, 2016).

All samples were analysed on a JEOL JXA-8530F (JEOL UK Ltd., Welwyn Garden City, UK) FEG-EPMA in the School of Earth Sciences at the University of Bristol running Probe for EPMA (PfE) analysis software (Probe Software Inc., Eugene, Oregon, USA). Measurements were made at 5, 7, 10, 15, 20 and 25 kV using either a 50 nA beam current with peak and background count times of 30 s and 15 s respectively or 25 nA and count times of 60 s + 30 s. The beam was defocussed to 10 μm which has been shown previously to suppress beam-induced C deposition or erosion (Matthews et al., 2018b). In addition, a Peltier cooled cold trap above the sample was maintained at about -26°C to further reduce any hydrocarbon cracking onto the sample surface (Buse et al., 2016). For each sample and accelerating voltage, a 4 x 3 grid of points with a point spacing of 20 μm was collected. The spectrometer conditions used are summarised in Table 2.

Spectrometer	Sp1	Sp2	Sp3	Sp4	Sp5
Crystal	LDE1	LDE2			PETL
Counter	P10	P10			Xe
Peak	O Kα	C Kα2			U Mα
BG offset	+20, -10	-19.5			±3
BG slope	Exp 8.0	1.00			-
RM	Fe_2O_3	Vit. C			UO_2

RM coating	Uncoated	Uncoated			15 nm C
Overlap		U			

Table 2   Spectrometer conditions used for analysis.

Vitreous carbon and a certified Fe_2O_3 (Astimex Standards Ltd., Toronto, Ontario, Canada), mounted in conductive phenolic resin, were used as C and O reference materials respectively. Fe_2O_3 has been identified as being sufficiently electrically conductive (Bastin & Heijligers, 1992) for both reference materials to be used uncoated.

Uranium calibrations were carried out using UO_2. A high pressure sintered powder UO_2 was first tried but this retained a significant level of porosity and calibration measurements needed to be manually filtered to reject data points suspected of being affected by this. A few fragments of synthetic UO_2 were donated for this project by the Natural History Museum (NHM reference number STD196), originally grown at the Berkeley Laboratories in California, USA, which proved to be fully dense and far more suitable as a calibration reference. The supplied fragments of synthetic UO_2 were mounted in conductive epoxy and calibration measurements made both without a conductive coating and with a C-coat. The coating was applied using an Edwards Auto 306 vacuum evaporator (Edwards Vacuum, Burgess Hill, UK) to deposit ~15 nm of carbon. The thickness was controlled using the orange colour-change of a polished brass witness block (Kerrick et al., 1973) co-located and coated simultaneously with the samples.

As described below, a correction for a uranium N-line overlap on the second order C Kα peak was required. The high purity (50 ppm C) U metal sample was used to measure the U N-line derived intensity at the second order C Kα spectrometer

position and the proportional intensity of this relative to the U Mα intensity calculated. Measurement of the U Mα peak on the sample was then used to subtract the corrected proportion from the measured intensity at the second order C Kα peak position. This is a standard method of overlap correction and is available in most EPMA analysis software for quantification of bulk samples. For the layered samples analysed in this study the overlap corrections were calculated manually.

3   Results

3.1   Surface Charging of UO_2

Secondary electron (SE) imaging of the uncoated UO_2 mount did not show any obvious signs of surface charging, indicating that it may be sufficiently electrically conductive to allow the material to be used uncoated. To quantitatively test for surface charging, measurements were made to determine the Duane-Hunt limit (Duane & Hunt, 1915). Figure 1 shows the Duane-Hunt cut-off values calculated from the measured EDS profiles using DTSA-II at 5, 7, 10, 15 and 20 kV column voltages. At each voltage the coated (crosses) and uncoated (circles) UO_2 values are compared against the mean ±1σ standard deviation ranges for measurements on vitreous C, U metal and Fe_2O_3 reference mounts, all of which are good electrical conductors. At each voltage the coated and uncoated UO_2 values closely agree with each other and also fall within the 1σ standard deviation ranges of the other reference materials. Thus, there is no indicated electrical charging effect for the uncoated UO_2.
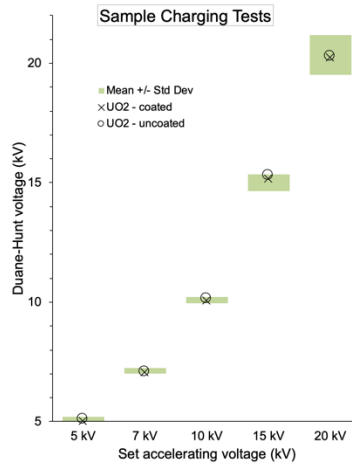
Figure 1   Duane-Hunt limit values for coated (crosses) and uncoated (circles) UO$_2$ compared to the mean and ±1σ standard deviation ranges (green boxes) of measurements on vitreous C, Fe$_2$O$_3$ and Bi metal at 5, 7, 10, 15 and 20 kV set voltages.

3.2   Measurement of Oxide Thickness

Uranium metal oxidises extremely readily in air. Growth of the first 10 nm is reported as following a logarithmic rate then transforming to a para-linear rate until the oxide is thick enough to spall (Chernia et al., 2006).

Linear coefficients, calculated using the linear parameterisation method developed in a previous paper (Matthews et al., 2018a), were used to determine the oxide thicknesses from measured O Kα k-ratios: Figure 2 shows O Kα k-ratios relative to Fe$_2$O$_3$ calculated using GMRFilm (Waldo, 1988) for 5, 10, 15 and 20 nm UO$_2$ layers on U at 5, 7, 10, 15 and 20 kV. The dashed lines show the best fit linear trends through the four layer thicknesses modelled at each voltage. R^2 goodness of fit values of better than 0.999 at all five modelled voltages show the high degree of fit between the modelled data points and the linear trends.
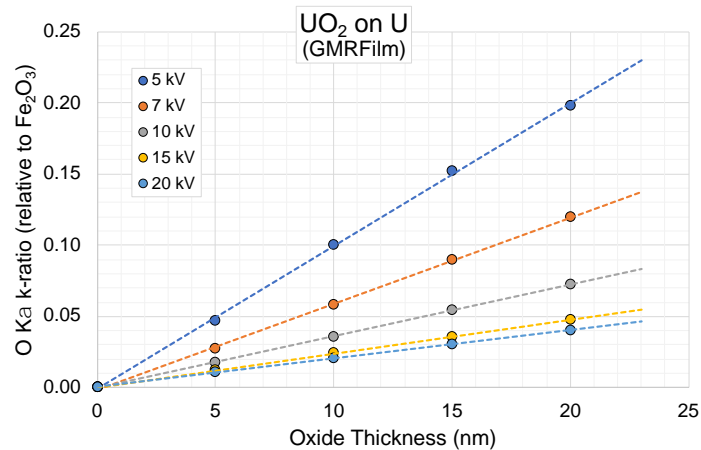
Figure 2   GMRFilm calculated O Kα k-ratios, relative to an Fe$_2$O$_3$ reference material, for 0, 5, 10, 15 and 20 nm

oxide thicknesses on U metal at 5, 7, 10, 15, and 20 kV. The dashed lines are linear fits through each

voltage dataset.

Figure 3 shows the results of a short series of air exposure experiments. The sample was first prepared using the final diamond polish and ethanol clean immediately before loading into the EPMA, with an effective air exposure time of ~20 s. The total air exposure time was then sequentially incremented between sets of repeat analyses at 5, 7, 10, 15, 20 and 25 kV by moving the sample to the instrument airlock and venting and opening the airlock door for measured time intervals. At each air exposure time the oxide thickness was calculated using GMRFilm from the O Kα k-ratios measured at the 6 accelerating voltages and assuming a stoichiometry of UO$_2$. The resulting values, averaged over the 6 voltages at each air exposure time, show a continuously increasing oxide thickness but with a decreasing rate of growth. A simple power curve of $y = 6.71.x^{0.11}$ gives a reasonably good fit to the measured data and shows the extremely rapid initial growth, with 10 nm of oxide forming after only ~20 s of air exposure.
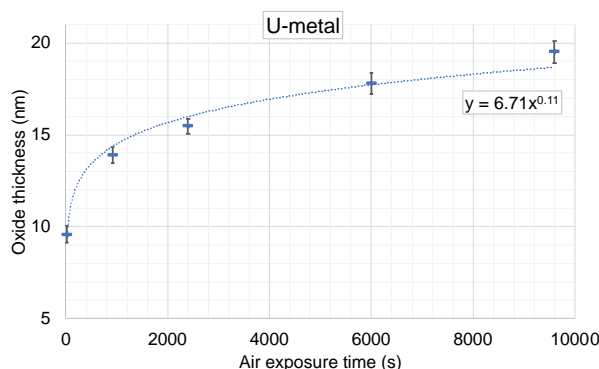
Figure 3   *Plot of measured UO_2 thickness grown on a polished uranium metal tile as a function of air exposure time. The vertical error bars show the $\pm 1\sigma$ standard deviation ranges. Thicknesses calculated from measured O $K\alpha$ k-ratios at 5, 7, 10, 15, 20 and 25 kV using GMRFilm.*

3.3 Oxide Valence State

Uranium oxide can exist in a wide range of valence states, and as both stoichiometric phases and solid solution ranges. A 1965 International Atomic Agency Report stated *"There are as many as 16 well-characterized uranium oxide phases, and the existence of a dozen more has been claimed."* (Holley, 1965). A more recent study declares "*…more than 20 phases existing as a function of temperature and pO_2 from UO_2 to UO_3"* (Skomurski et al., 2013). Figure 4 shows a portion of the U-O binary phase diagram from a 2002 PhD thesis (Busker, 2002) covering the range from UO_2 to U_3O_8. At room temperature this portion of the phase diagram shows the solid solution phases UO_{2+x} and U_4O_{9-y} and the stoichiometric phases U_3O_7, and U_5O_{13}. Air-grown oxide surfaces on uranium metal favour a close to stoichiometric UO_2 state at room temperatures and pressures (Allen et al., 1976; Bera et al., 1998; McEachern & Taylor, 1998; Senanayake et al., 2005). At the oxide-metal interface the oxide may be a sub-stoichiometric UO_{2-x}, whilst at the oxide-air interface hyper-stoichiometric UO_{2+x} can continue to absorb oxygen up to a maximum of x=0.25, at which point U_4O_{9-y} can form (Chernia et al., 2006).
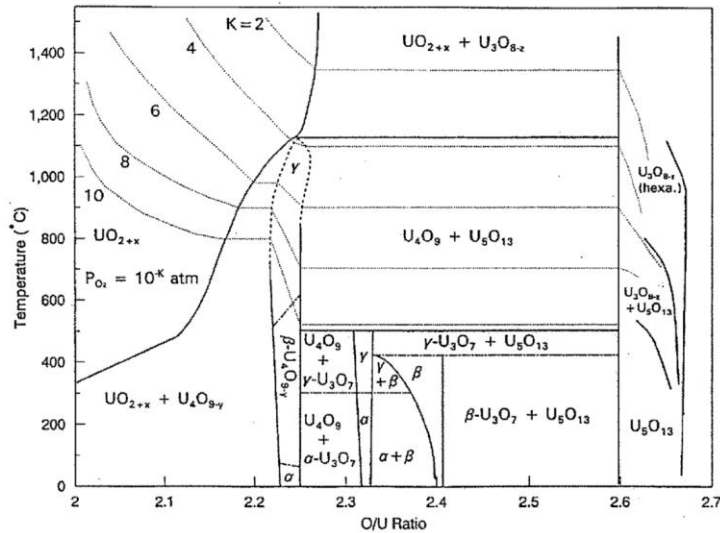
Figure 4   Portion of the U-O binary phase diagram showing some of the possible uranium oxide compositions and composition ranges. From Busker (2002).

The sensitivity of the substrate quantification to the assumed oxide stoichiometry was assessed with GMRFilm, using the 5 kV EPMA data, corrected for an 11 nm RM carbon coating, over a wide range of O:U atomic ratios. The results are summarised in Figure 5. Increasing the proportion of O decreases the resulting U content of the substrate. The changes are very small, with the U content only being changed by 0.65 wt% from 100 wt% for UO_2 to 99.35 wt% for a stoichiometrically extreme and chemically unlikely UO_{12}.
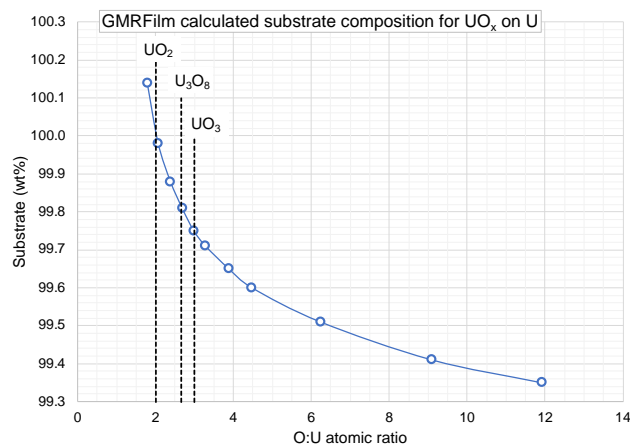

Figure 5   Substrate composition as a function of surface oxide stoichiometry relative to 100% for UO_2.

15

These results show that, even if the oxide layer is not homogeneous or stoichiometric UO_2 the effect on the substrate quantification is small.

3.4 Correction for Reference Material Coating

Calibration measurements were carried out on the UO_2 reference material both with and without a conductive carbon coating. As for the oxide layer on the U metal above, a C-coating can significantly reduce the measured k-ratio from the coated material, in particular at low accelerating voltages. Using the same methodology as for the UO_2 on U model the C Kα, O Kα and U Mα k-ratios and linear coefficients were calculated for a C on UO_2 model. Figure 6 gives the resulting plots or C Kα and U Mα. The measured C Kα ratio and coefficients at a given accelerating voltage are used to calculate the coating thickness and this in turn to calculate the reduction in the U Mα k-ratio. The C-coated UO_2 k-ratios in Figure 6b were calculated relative to an uncoated UO_2 so the given k-ratio values are equivalent to the proportional change in intensity of the U Mα as a result of the C-coating on the UO_2 RM. This proportional change can thus be used to derive corrected k-ratios for the sample analyses. For example, a measured C Kα k-ratio at 5 kV of 0.45 on the UO_2 RM gives a calculated 10 nm C coating thickness (shown by the red arrows in Figure 6a). This coating thickness reduces the measured U Mα k-ratio to 0.89 relative to an uncoated UO_2 (shown by the red arrows in Figure 6b). The uncorrected sample k-ratio, k = sample intensity/RM intensity, is increased by this proportional reduction in the RM U Mα intensity. Multiplying the sample k-ratio by 0.89 corrects it to being relative to an uncoated RM.
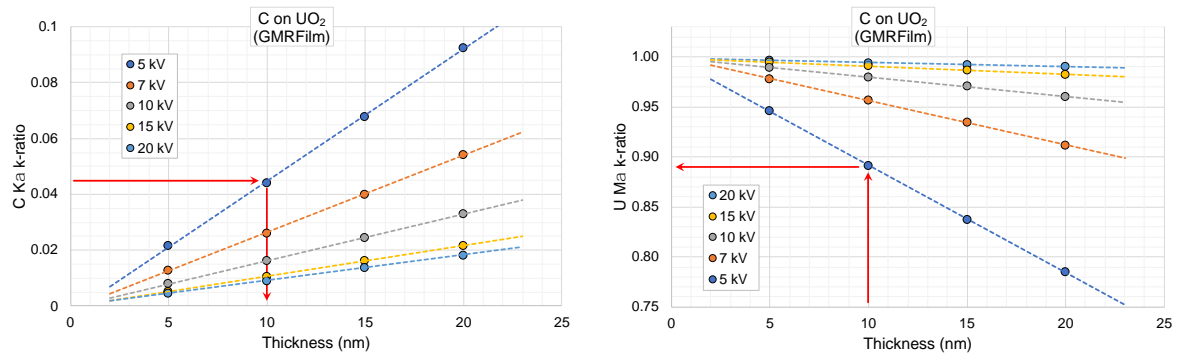
Figure 6   GMRFilm calculated a) C Kα k-ratios relative to vitreous C, and b) U Mα k-ratios relative to uncoated UO₂, for 5, 10, 15 and 20 nm oxide thicknesses on U metal at 5, 7, 10, 15, and 20 kV. The dashed lines are linear fits through each voltage dataset. For an explanation of the red arrows see the main text.

3.4.1   Measurement of Carbon with Uranium

The University of Bristol JEOL FEG-EPMA offers a choice of diffraction crystals capable of measuring the C Kα x-ray line. The LDE2 layered diffracting element (2d = 10 nm) provides the highest intensity but lowest resolution, with a FWHM of 14.8 eV measured on a vitreous carbon RM. A C Kα peak scan on a UC inclusion appears to show a single peak shifted +40 eV relative to the vitreous C but Figure 7 shows that this apparently single peak is the superposition of two closely spaced peaks: A peak scan on a carbon-free uranium metal sample reveals an uranium peak with ~80 eV higher energy than the C Kα peak on the vitreous carbon. Subtracting this signal from that measured on the UC leaves a residual peak coincident with the vitreous carbon peak position.
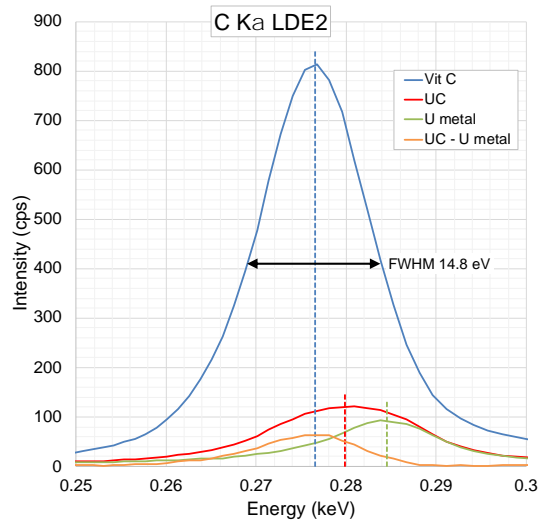
Figure 7   X-ray spectral plots in the energy range of the C Kα peak measured using an LDE2 layered diffracting element on vit. C, UC and high purity uranium metal showing that the residual of the UC signal after the U-metal signal is subtracted is a peak coincident with the vit. C peak position.

Neither PfE nor the JEOL software tools identified any U lines in the energy region of the C Kα peak[1], but inspection of the Bearden (1967) x-ray tables, an extract of which is given in Table 3, shows the U N_6-O_4 line has an energy of 0.286 eV, which agrees with the U-metal peak position in Figure 7. Note that the original paper lists this line as the N_4-O_4 line but a check of the absolute sub-shell energies in Bearden and Burr (1967) show this is a misprint. The Bearden tables also list an N_6-O_5 line at 0.294 eV but which is not evident in the scans in Figure 7. It is assumed the intensity of this peak is too low to be revealed in these plots.

U transition	Energy (keV)
N_6-O_4	0.286

---

[1] An investigation of the PfE data tables indicates that they do not include transitions beyond the M-shells.

N_6-O_5	0.294
N_5-N_6	0.356
N_4-N_6	0.390

Table 3   Energies of U-lines in the region of the C $K\alpha$ peak. From Bearden (1967).

The interference can be accounted for using an overlap correction, but the tail of the U line under the C $K\alpha$ peak position, as shown by the U metal profile in Figure 7, is roughly the same magnitude as the C $K\alpha$ component in the UC when measured with an LDE2 diffracting element and thus the correction would be large.

The energy range of the LDE1 layered diffracting element (2d = 6 nm) also covers the C $K\alpha$ peak position. As Figure 8 shows, it provides an improved FWHM on the vitreous C of 11 eV but with less than a 20th of the intensity of the LDE2. The UC peak scan now indicates the two superimposed peaks, but the resolution is still insufficient to separate the C $K\alpha$ signal from the U N-line.
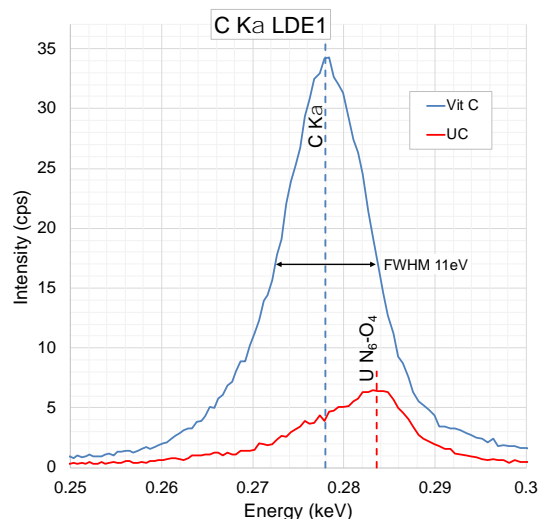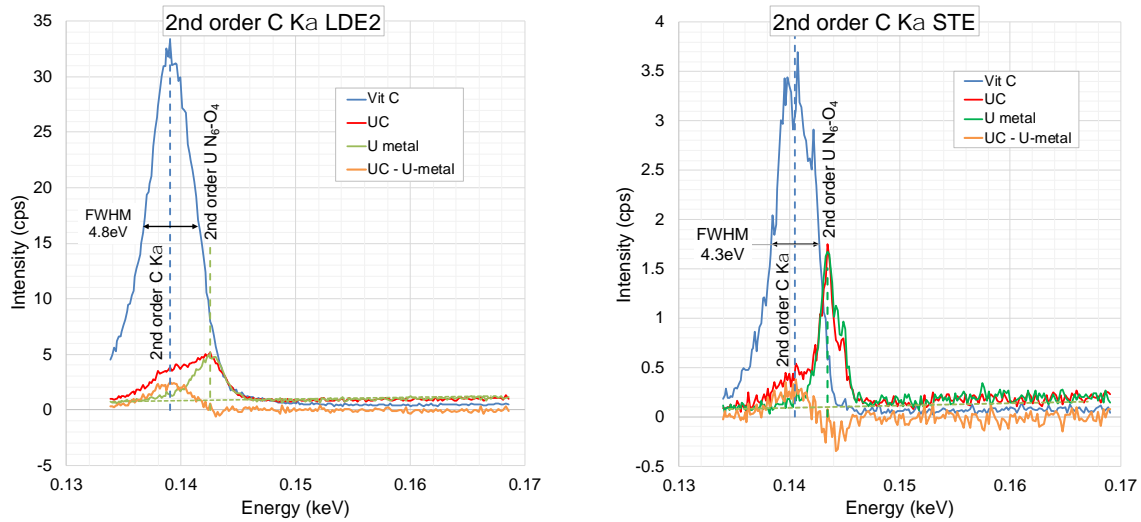

Figure 8   X-ray spectral plot in the energy range of the C $K\alpha$ peak measured with an LDE1 diffraction crystal on vitreous carbon (Vit. C) and uranium carbide (UC).

A further improvement in resolution can be achieved by utilising the 2nd order C Kα peak. Since this is measured at a spectrometer position equivalent to double the wavelength and half the energy of the first order peak this lies at the low energy end of the spectrometer range for the LDE2 diffracting element. For Johann geometry diffracting crystals resolution increases as energy decreases along the spectrometer range (Matthews, 2016). Figure 9a shows the spectral scans on vitreous carbon, UC, U metal, and the residual of the U metal profile subtracted from the UC values. The truncation of the low energy tails of the peaks in this figure are caused by the low energy limit of the spectrometer range. The intensity of the vitreous C peak is the same as for the first order peak on the LDE1, but the FWHM is significantly reduced to 4.8 eV. The peak differentiation is marginally improved relative to the first order LDE1 spectra, but still insufficient to fully separate the overlap. A further small improvement in resolution is provided by a lead stearate, STE, diffracting element (2d = 10 nm), with a FWHM on the 2nd order C Kα of 4.3 eV, but this marginal change doesn't provide any tangible improvement in the peak separation and the intensity is reduced to ~1/10th that of the first order peak on the LDE1 and 1/200th of that on the LDE2.

Whilst overlap correction cannot be avoided, the magnitude of correction on the LDE2 is considerably reduced to only ~10% of the measured C Kα signal by the higher resolving power at the 2nd order peak positions and this configuration was therefore selected for all analyses. The spectrometer range limit also requires the background intensity to only be measured on the high energy side of the peak, with a slope factor of 0.74 used to extrapolate the intensity under the peak. The calculated background slopes for the U-metal data for both the LDE2 and STE crystals are shown by the green short-dashed lines in Figure 9.

Figure 9   X-ray spectral plots in the energy range of the second order C Kα peak measured vitreous carbon (Vit. C) and uranium carbide (UC) using a) LDE2, and b) lead stearate diffracting crystals. The calculated background slopes for the U-metal data is shown as the green short-dashed lines in both figures.

To test the magnitude of the overlap interference, 6 analyses were carried out on a C-free U metal at 10 kV and the results quantified both with and without the U overlap correction applied. Analysis conditions used were those shown in Table 2 above and the results are summarised in Table 4. The corrected results are fixed at 0 wt% C since the overlap correction was calculated from calibration measurements made on the same C-free U metal, but the uncorrected analyses show a C content of almost 1 wt% and an analysis total of 101.3 wt%. due to the contribution from the U N_6-O_4 line.

U metal (wt %), 10 kV	C	U	Total
No U overlap correction	0.97 ± 0.03	100.32 ± 0.14	101.29 ± 0.16
With U overlap correction	0.00 ± 0.02	100.00 ± 0.14	100.00 ± 0.16

3.5   O Kα and U Mα Mass Absorption Coefficient Values in UO$_2$

The P&P MAC measurement method was applied to measurements carried out in this study for O Kα and U Mα absorption in UO$_2$, using Casino (Drouin et al., 2007) and PENEPMA (Llovet & Salvat, 2016) to calculate the theoretical intensity versus accelerating voltage values. To get a meaningful measure of the MAC values it is necessary for any sample artefacts or structures, such as a conductive coating or surface oxide, to be fully corrected for. Corrections for the carbon coating on the UO$_2$ were calculated using the linear parameterisation method described above and applied to the measured intensities. Pöml and Llovet (2020) compensated for the Al coatings used in their study by applying a correction factor to their measured intensities equal to the theoretical decrease in intensity per unit of measured Al coating thickness. This is equivalent to the linear parameterisation method used here.

The resulting intensity versus voltage plots and derived MAC values for U Mα and O Kα absorption in UO$_2$ using PENEPMA are shown in Figure 10 whilst Table 5 summarises the compound MAC values calculated from both Casino and PENEPMA. The O Kα absorption, as a result of its very low energy, is an order of magnitude greater than for U Mα and this MAC, and any associated errors, will dominate the quantification correction.
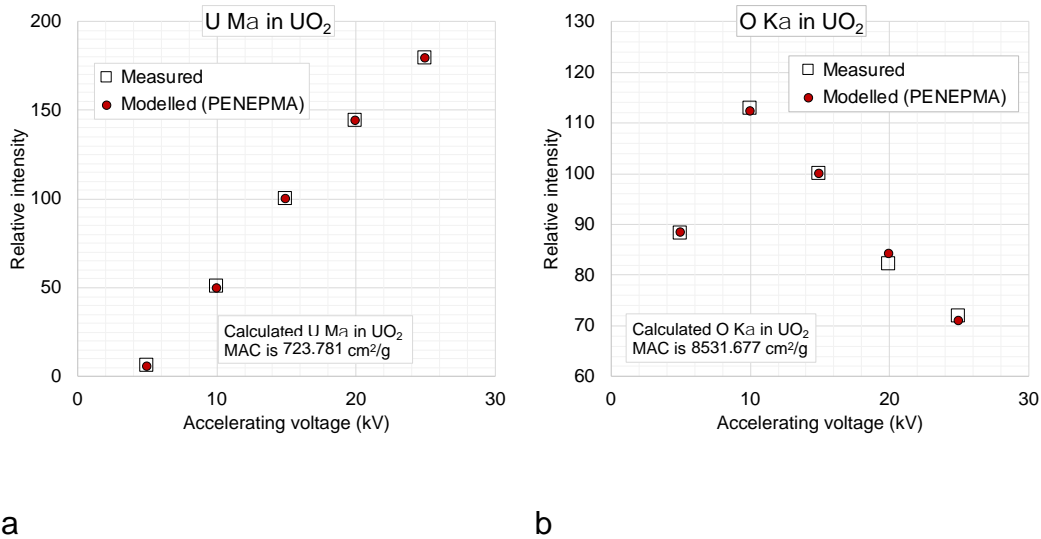
Figure 10 Plots of relative intensity versus accelerating voltage and calculated MAC values for a) U Mα in UO$_2$,

and b) O Kα in UO$_2$.

Compound MAC in UO$_2$ (cm^2/g)	O Kα	U Mα
Casino	8214	899
PENEPMA	8532	724

Table 5   Measured compound MAC values for O Kα and U Mα in UO$_2$ using Casino and PENEPMA.

To calculate the elemental MACs for O Kα absorption by O and by U from the

compound O Kα in UO$_2$ MAC a simple lever rule is applied:

$$z = ax + by$$

Equation 3

where *z* is the O Kα absorbed in UO$_2$ compound MAC

x is the O Kα absorbed by U MAC

y is the O Kα absorbed by O MAC, and

a and *b* are the weight fractions of U and O in UO$_2$ respectively.

The O Kα and U Mα absorbed by O MACs are assumed to be well characterised since published values show relatively little variation. Using the FFAST (2005) database values of 1120 cm^2/g and 175 cm^2/g respectively the O Kα absorbed by U MAC values are calculated from the measured Casino and PENEPMA compound MAC values as 9168 cm^2/g and 9528 cm^2/g respectively. Figure 11 compares these values against other published values. These range from 5260 cm^2/g (Henke et al., 1993) to 14021 (Ruste & Gantois, 1975), a factor of almost 3 difference, demonstrating how poorly constrained this MAC value is. The CASINO and PENEPMA-derived values from this study both compare very closely to Pöml & Llovet's (2020) experimentally derived value of 9318 cm^2/g.
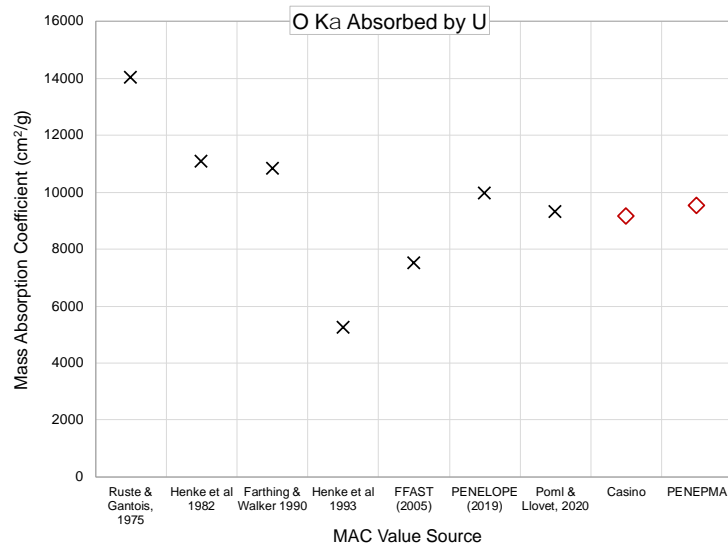
Figure 11 Comparison of MAC values for O Kα in U. Black crosses are previously published values whilst the red diamonds are calculated from O Kα measurements in UO$_2$ in this study.

Pöml and Llovet (2020) also presented Monte Carlo derived MAC values, shown as the 'PENELOPE (2019)' datapoint in Figure 11. These were calculated from the TABLE program, distributed as part of the PENELOPE Monte Carlo software package (Salvat, 2015), which derives MAC values from the cross-sections of the

three primary processes that produce absorption: photo-ionisation, Compton (inelastic) scattering, and Rayleigh (elastic) scattering. The three sets of cross-sections, and the resulting MAC values, are derived almost entirely from first principles and are therefore free from experimental measurement errors and artefacts. This produced an O Kα absorbed by U MAC of 9962 cm^2/g. This is less than 10% higher than the values measured in this study and gives a level of confidence that these values are not unrealistic.

The GMRFilm default MAC values for U Mα and O Kα absorbed by U, shown in Table 6, differ from the P&P-with-PENEPMA method calculated values by -10% and 12% respectively. To determine the magnitude of effect these differences have the UO_2 on U models and sample quantifications were re-calculated using the P&P method derived MAC values. As described above, FFAST MAC values for U Mα and O Kα absorbed by O were used to derive the U Mα and O Kα in U MAC values from the measured U Mα and O Kα in UO_2 MACs so the FFAST values were again used as part of the recalculation. The full set of GMRFilm and modified MAC values are summarised in Table 6.

Line	Absorber	GMRFilm	Modified
U Mα	U	720.83	797.57[C]
	O	183.09	174.87[F]
O Kα	U	10869.74	9528.06[C]
	O	1180.70	1120.43[F]

Table 6   Default MAC values used by GMRFilm and MAC values used for recalculation of the models to

incorporate the U Mα and O Kα absorbed by U MACs (denoted by superscript 'C') determined using

Figure 12 shows the percentage difference in substrate compositions at 5, 7, 10, 15, 20 and 25 kV using the P&P method derived MAC values from those calculated using the GMRFilm default MAC values. The change in substrate composition is small, ranging from a 0.45% increase relative to the default MAC value compositions at 25 kV to no difference at 5 kV. The influence of the MAC decreases with decreasing accelerating voltage since the x-ray path lengths and therefore degree of absorption both decrease as the voltage decreases.
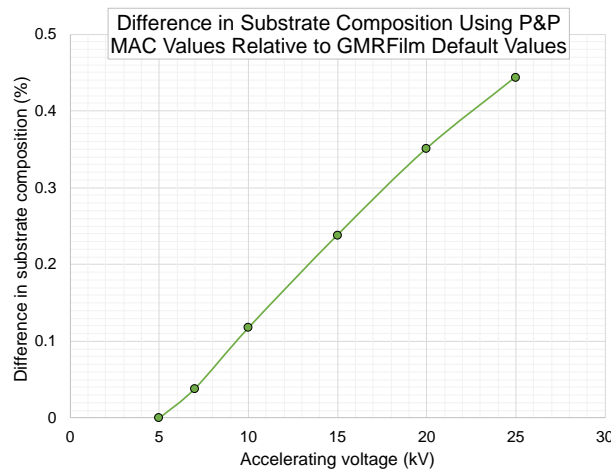
Figure 12 Difference in substrate compositions calculated with GMRFilm using P&P method derived MAC values relative to those calculated using the GMRFilm default values.

3.6   Experimental Measurements on U-metal

Figure 13 and Figure 14 summarise both modelled and measured O Kα and U Mα k-ratios respectively, analysed at 5, 7, 10, 15, 20 and 25 kV on an uncoated high purity U metal sample. 1σ standard deviations for the EPMA data are approximately the size of the 'X' symbols used in the plots. Using the O Kα k-ratios, calibrated relative to Fe_2O_3, the oxide thickness was calculated to be 10.0 ± 0.7 nm and 12 ± 1.2 nm

using GMRFilm and PENEPMA derived linear coefficients respectively. In Figure 13 the measured k-ratios at each voltage are compared against the GMRFilm modelled values for 0, 5, 10, 15 and 20 nm UO_2 on U but the PENEPMA modelled values were very similar. Both GMRFilm and PENEPMA predict similar O Kα k-ratios for each set of conditions and the EPMA results correlate closely with the 10 nm oxide thickness curves over all the measured voltages.
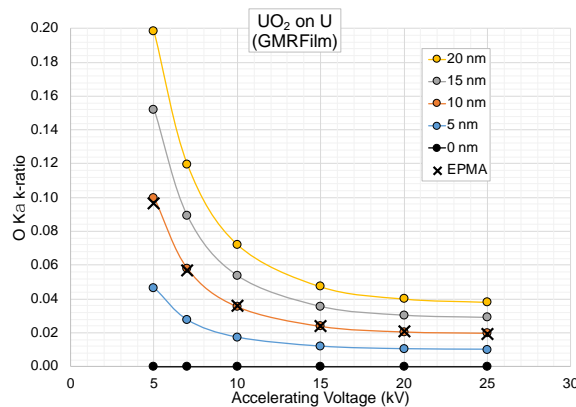
Figure 13 EPMA O Kα k-ratios measured at 5, 7, 10, 15, 20 and 25 kV compared to GMRFilm calculated values for a 0, 5, 10, 15 and 20 nm UO_2 on U model.

Figure 14a and b show the GMRFilm and PENEPMA calculated U Mα k-ratios for the UO_2 on U model for 0 – 20 nm UO_2 layers. In each plot the EPMA k-ratios measured relative to a carbon coated UO_2 are overlaid. Measurements of the C Kα k-ratio on the UO_2 RM in combination with the calculated linear coefficients gave a coating thickness of 11 ± 1 nm from both GMRFilm and PENEPMA. Variation in calculated thickness was found to be greater between accelerating voltages than between measurements at a given voltage, ranging from a minimum of 9.63 ± 0.04 nm at 10 kV to a maximum of 11.94 ± 0.72 nm at 25 kV. EPMA k-ratios both with and without correction for the carbon coating are shown. The C-coating corrected values at each accelerating voltage were calculated using the measured C-coating

thickness at that voltage. Applying the ± 1σ ranges in the C-coating thicknesses

changed the resulting U Mα k-ratio values by less than the size of the 'X' symbols
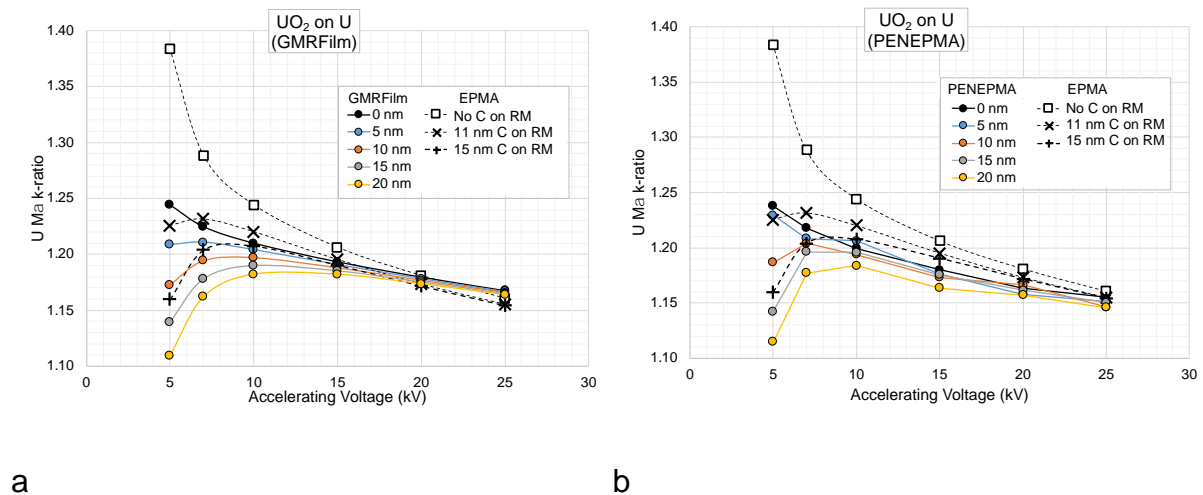
used to plot the data in Figure 14.

a   b

Figure 14 Comparisons of U Mα k-ratios, both uncorrected and corrected for 11 nm and 15 nm C coatings on the
RM, to calculated values for 0, 5, 10, 15 and 20 nm UO2 on U models using a) GMRFilm, and b)
PENEPMA at 5, 7, 10, 15, 20 and 25 kV.

The change from steadily increasing x-ray intensities with decreasing voltage in the

unoxidized metal to increasing then decreasing for the oxidised model, can be

explained by reference to the depth distribution, $\phi(\rho z)$, curves. Figure 15 shows $\phi(\rho z)$

curves calculated using the Monte Carlo software Casino (Drouin et al., 2007) for the

10 nm of oxide model at 5, 7, 10, 15, 20 and 25 kV accelerating voltages. Each

curve shows the typical $\phi(\rho z)$ shape, increasing from a surface intensity value to a

maximum at some depth below the surface and then decreasing to the ultimate limit

of x-ray emission. The depth of the intensity maximum and the maximum depth of

emission both increase with accelerating voltage. The changes from increasing to

decreasing intensities in Figure 14 occur at the voltages where the $\phi(\rho z)$ maximum

crosses the oxide-metal interface. For the 10 nm oxide thickness model shown in

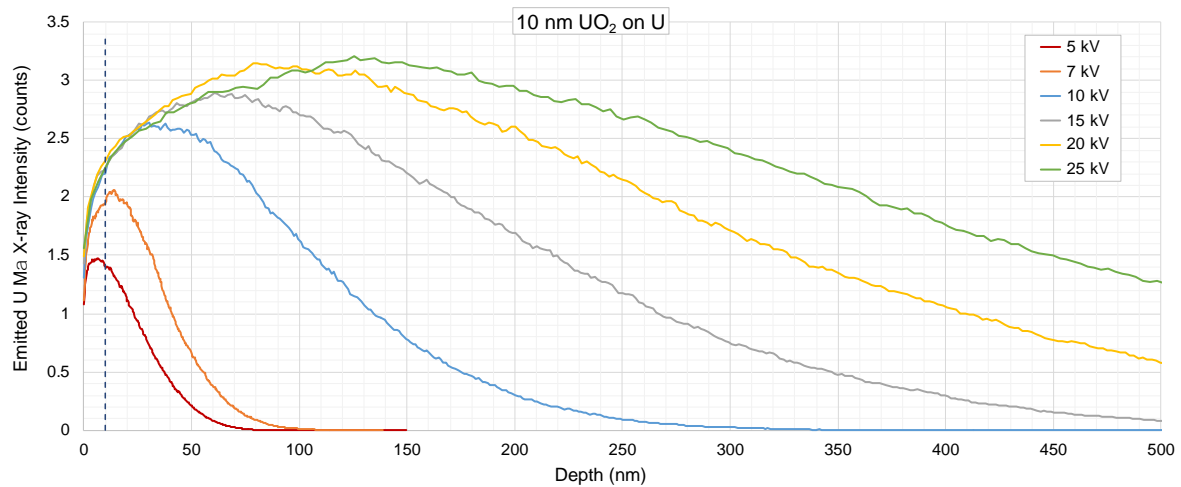Figure 15 this is at about 7 kV, which correlates with profile for the 10 nm oxide model curve in Figure 14.

Figure 15 $\phi(\rho z)$ depth distribution curves modelled using Casino v 2.5.1.0 (Drouin et al., 2007) for a 10 nm UO$_2$ layer on U metal. The vertical dashed line indicates the position of the oxide-metal interface.

Above 15 kV in Figure 14 neither the oxide on the sample nor the C-coating on the RM have much influence on the U Mα k-ratio. The EPMA data agrees reasonably well with the GMRFilm model data at these voltages (Figure 14a), although the model doesn't predict as strong a decrease in k-ratio with increasing accelerating voltage as measured on the sample. The PENEPMA model, Figure 14b, predicts lower k-ratio values than both the GMRFilm model and the measured values.

Decreasing the voltage below 15 kV produces progressively greater deviations of the uncorrected EPMA datapoints above both the GMRFilm and PENEPMA modelled data. At 5 kV the uncorrected EPMA k-ratio of 1.38 is ~18% greater than the GMRFilm predicted k-ratio for the 10 nm oxide indicated by the O Kα measured k-ratio, and ~11% higher than a completely oxide-free U metal. Applying the correction for the carbon coating on the RM reduces the EPMA k-ratios but not sufficiently to fully agree with the modelled data: The curvature of the corrected EPMA data at low

kV lies between those of the 5 nm and 10 nm oxide model data for both models, but the absolute values for the EPMA k-ratios are still higher than either models.

Whilst the EPMA measured C Kα k-ratios give a carbon coating thickness of 11 nm, the colour of the polished brass witness block coated simultaneously with the UO_2 RM indicated the thickness to be ~15 nm. Applying a correction for this thicker coating value on the RM brings the EPMA data into better agreement with the 10 nm oxide data for the GMRFilm model (Figure 14a), but closer to 15 nm oxide values using the PENEPMA model values (Figure 14b).

The magnitudes of influence that the oxide layer and the RM coating have on the accuracy of analyses can be gauged from the percentage differences between the uncorrected and corrected values and the predicted model values. The percentage difference can be used as measure of the error in the parameter measurement.

Figure 16 gives the percentage differences of the U Mα k-ratio from the GMRFilm and PENEPMA calculated models. The potential errors increase rapidly with decreasing accelerating voltage. With no corrections applied for either the carbon coating on the RM or the oxide layer on the sample (grey squares) the error is 11% at 5 kV. The effect of the oxide layer is to decrease the measured k-ratio so correcting only for the oxide thickness as determined from the measured O Kα k-ratios (grey circles) increases the k-ratio and thus further increases the error from 11% to 18% at 5 kV. The RM coating, by decreasing the intensity measured on the RM, increases the k-ratio on the sample. Applying the C-coating correction without the oxide correction results in an error of between -2% and -7% at 5 kV, depending on whether the EPMA measured C thickness of ~11 nm (blue squares) or 15 nm (orange squares) is used. The relative impact of this correction is significantly greater

than the oxide correction: The oxide correction changes the percentage difference by 7% whilst the C-coating correction effect is between 13% and 18%. Combining both corrections results in an error range at 5 kV of -1% to 5%. The best fit is provided by the oxide correction in combination with the 15 nm C coating (orange circles), as indicated by the colour change of the brass witness block, rather than with the C coating thickness determined from the C Kα measured k-ratios (blue circles).
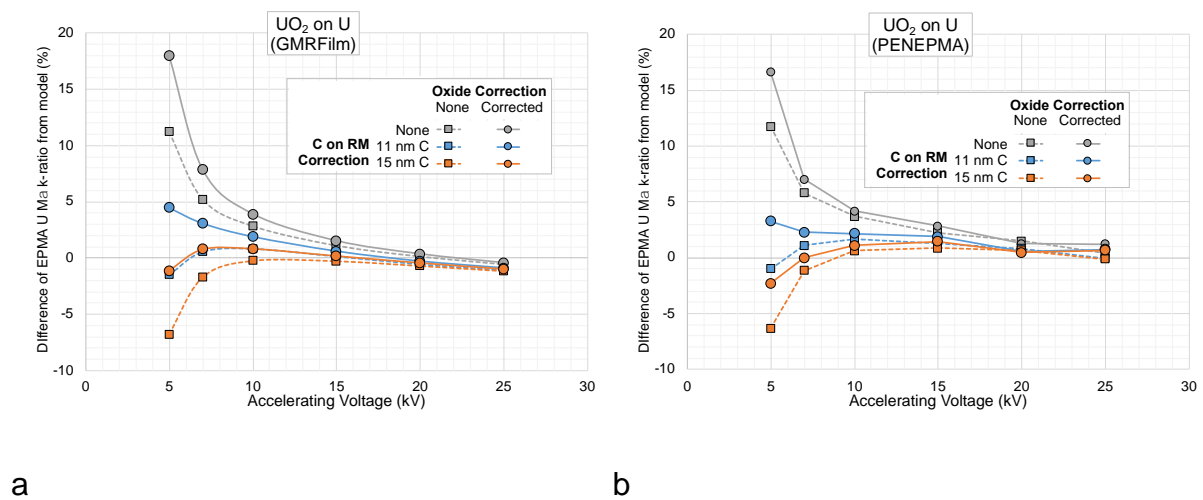
Figure 16 Percentage differences between the EPMA measured U Mα k-ratios and a) GMRFilm, and b) PENEPMA modelled values showing the relative impacts of the sample oxide and RM carbon coating corrections.

One of the purposes of determining the oxide layer thickness is to allow for the measurement of the true sample composition under the oxide. For this the component of the U Mα k-ratio derived from the substrate needs to be determined. GMRFilm outputs both the substrate and oxide layer i-ratio components of the U Mα k-ratio. Subtracting this oxide i-ratio from the EPMA measured k-ratio leaves the residual substrate i-ratio component of the EPMA measurement. Figure 17a shows the percentage differences between the EPMA substrate i-ratio values and the directly calculated GMRFilm substrate i-ratios with and without the oxide and RM

coating corrections. At 5 kV the error range is ±30%, with the largest errors incurred by applying only one of the two corrections: Correcting for the oxide but not the RM coating (grey circles) increases the error from -11% with no corrections (grey squares) to 29%, a change of 40%. Correcting for the RM coating but not the oxide (blue squares and orange squares) increases the no-correction error by 19%, from -11% to about -30%.

The difference in error between the 11 nm and 15 nm coating corrections for the substrate is smaller than for the U Mα k-ratio values shown in Figure 16, and the influence of the coating correction (19% at 5 kV) is smaller than that of the oxide layer (40% at 5 kV). The best fit is again provided by the oxide correction in combination with the 15 nm RM C-coating correction, with an error of only 1% at 5 kV. These error magnitudes are confirmed by direct thin film quantification using GMRFilm, as shown in Figure 17b and Table 7. Correction for the oxide layer is included in the thin film quantification algorithm so the curves plotted in Figure 17b are equivalent to the oxide corrected curves in Figure 17a. Analyses at 10 and 15 kV calibrated using an uncoated UO_2 RM are also shown for comparison. Values shown in red in the table lie outside an arbitrarily set acceptable analysis error range of 100 ± 1%.
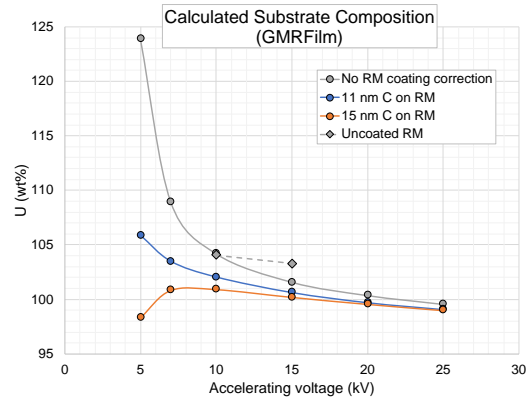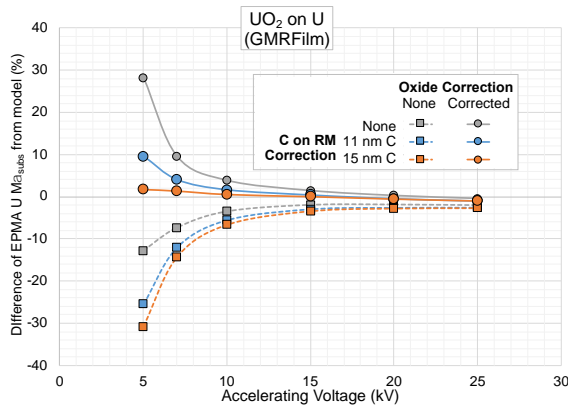
a   b

Figure 17 a) Percentage differences between the calculated EPMA U Mα substrate i-ratios, and b) comparison
of substrate compositions calculated using GMRFilm as a result of different RM coating corrections
applied.

The magnitudes of the errors agree well with the percentage differences in Figure
17a, with the 15 nm C-coating correction (orange circles) providing the best results.
Without correction for the RM coating (grey circles), only analyses at 20 and 25 kV
produce acceptable analyses. Attempting such analyses at 5 kV incurs errors of
nearly 25%. Applying a correction for the ~11 nm coating thickness determined from
the C Kα k-ratio (blue circles) reduces the error at 5 kV to ~6% but only provides
acceptable analyses down to 15 kV. The correction for a 15 nm C on the RM (orange
circles) produces the most consistently acceptable analyses down to 7 kV, but with
an over-correction of nearly 2% at 5 kV.

GMRFilm	Accelerating voltage (kV)					
RM correction	5	7	10	15	20	25
None	123.9	109.0	104.2	101.6	100.4	99.6
11 nm C	105.9	103.5	102.1	100.6	99.7	99.1

15 nm C	98.3	100.8	100.9	100.2	99.6	99.0
Uncoated RM			104.1	103.3		

Table 7   GMRFilm calculated substrate compositions for the oxidised U metal sample with and without

corrections applied for the RM coating. Values in red fall outside an acceptance range of 100 ± 1%.

The uncoated RM failed to provide acceptable analyses at either 10 or 15 kV. Indeed, the 15 kV analyses are ~2% poorer than the uncorrected analyses on the C-coated RM.

4   Discussion

Correcting for the RM coating and sample surface oxide reduces but doesn't completely remove the significant analysis error at low accelerating voltages. The non-zero slope of the corrected curves in Figure 17b implies a residual systematic error. The results for the sample surface oxide and 15 nm C on RM corrected values produce acceptable substrate compositions above ~6 kV but the data shows a strong decreasing trend in values below ~7 kV, producing an error of over -1.5% at 5 kV and implying increasingly larger errors at lower voltages.

4.1   Reference Material Coating

The need to correct for the RM conductive coating at low analysis voltages is clearly demonstrated above. The thickness derived from the C Kα k-ratio produced a value only ~70% that of the 15 nm determined optically at the time of deposition and this made the difference between a 98% (15 nm C) and 106% (11 nm C) analysis total. The colour-change thickness determination method can be very accurate: The colour is produced by the interference between the light reflected from the upper and lower surfaces of the coating and is a function of the thickness and refractive index of the

coating material. Since the latter is a fixed value for a given coating material the colour is therefore a direct function of the thickness. The main limitation is the ability of the human eye to repeatably distinguish the colour shade. The poorer accuracy of the C Kα k-ratio calculated thickness can perhaps be attributed to the need to correct the measured C Kα intensity of the U N$_6$-O$_4$ overlap. The comparison does show that accurate determination of the coating thickness has a significant impact at low accelerating voltages. The results in Table 7 support the optically measured thickness as being more accurate, but the residual error could be attributed to this still not being accurate enough.

Coating both the sample and reference material would have removed the need to correct the reference material intensities but would have required modelling the sample as a 3-layer coating-on-oxide-on-substrate system. A 3-layer modelling method has been demonstrated in a previous publication (Matthews et al., 2019) but the resultant errors in that study are comparable to the method used in this study of combining 2-layer modelling of both the sample and the RM.

The Duane-Hunt measurements indicated that UO$_2$ is sufficiently electrically conductive to allow for it to be used uncoated. However, the test analyses failed to produce acceptable results. The Duane-Hunt limit is not an infallible measure of sample charging. In particular it relies on the surface charge build-up being very rapid compared to the spectrum acquisition time (typically 10's of seconds). For highly insulating materials this is commonly the case but for poorly electrically conductive materials there may be a more gradual charge build-up. In this case the slowly reducing cut-off value could be obscured in the time integrated EDS spectrum. Progressive charge build-up could be tested for by dividing the EDS acquisition time into sub-intervals and checking for drift in the cut-off voltage but this

time slicing method is limited by the very low signal level intrinsic to measuring the cut-off to zero counts. The low signal level also imposes a limit to the energy resolution of the method. From Figure 1 the 1σ range is approximately ±10%. However, it is expected that SE imaging would show even a slow charge build-up and this was not seen, supporting the Duane-Hunt evidence that the UO_2 is sufficiently electrically conductive. The reason for the poor performance of the uncoated UO_2 is not yet understood and requires further investigation.

A previous study (Matthews et al., 2018b) showed that electron beam induced carbon accumulation or erosion can significantly change the thickness of a C-coating during a 60 s analysis, and that this can have a measurably adverse effect on substrate quantification. However, that study also demonstrated that a 10 μm defocussed electron beam in combination with Peltier cooled cold trap (Buse et al., 2016), as was used in this study, was highly effective at suppressing these processes at voltages down to 5 kV so this is not deemed to be a significant factor here.

Aluminium is a potential alternative coating since it is not prone to beam induced erosion, doesn't require overlap correction, and also has a lower MAC than C for soft x-rays (Love et al., 1974; Bastin & Heijligers, 1991), thus requiring a smaller correction for a given coating thickness. However, it has been previously reported (Matthews et al., 2018a) that determination of and correction for Al coating thicknesses can be problematic. In particular, quantification errors at 5 kV of 10 – 20% for an Al coated Bi metal substrate were reported in that study, an order of magnitude poorer than the ~2% overcorrection for the C coating at 5 kV. Pöml and Llovet (2020) did not experience the same level of errors with their Al coating

corrections, but still reported differences between their coating corrected and theoretical MAC values of ~4%.

4.2 MAC Values

A limitation of the P&P MAC calculation method is that it assumes that the theoretical changes in x-ray intensity with accelerating voltage are accurate, and that any differences between the calculated and measured intensities are entirely due to the MAC value. However, the O Kα and U Mα in U MAC values calculated above agree well with recent publications and the differences from the default values in GMRFilm are small enough to have only a small impact on the substrate quantification, as shown in Figure 12. This figure also shows that the influence of the MAC decreases with decreasing accelerating voltage: As the voltage is reduced the electron and x-ray path lengths in the sample decrease so the amount of absorption also decreases. This should not be confused with greater MAC value uncertainties that result from the need to use lower energy x-ray lines in order to analyse at lower voltages.

4.3 Model Fidelity

PENELOPE (Salvat, 2015), the Monte Carlo engine on which PENEPMA (Llovet & Salvat, 2016) is based, is considered to be a 'high fidelity' modelling engine: The atomic interactions are calculated from first principles and should represent the true electron-sample interaction as closely as is possible from our current understanding of the physical processes. A consequence of this fidelity is a high computational overhead and a single thin film model at a given accelerating voltage can take several hours to complete. GMRFilm (Waldo, 1988) uses a $\phi(\rho z)$ quantification algorithm, with look-up tables based on historic data for the correction factors and

ionisation cross-sections etc… to iteratively calculate either the compositions and thicknesses from input k-ratios, or k-ratios from input compositions and thicknesses. A model takes only a few seconds to calculate using this lower fidelity program.

The two programs do show differences, but PENEPMA doesn't necessarily produce more accurate results. For example, Figure 16 shows that both models can reduce the errors in the EPMA measured U Mα k-ratios to 1 – 2% at 5 kV but whilst PENEPMA has smaller residual errors than GMRFilm at 25 kV they are larger at 10 kV. Model fidelity cannot, therefore, account for the residual systematic errors. This should not be entirely surprising. The equations and look-up tables that GMRFilm uses are built from a combination of theory and experimental values so the calculated values should predict experimental results reasonably well. That GMRFilm and PENEPMA produce similar but inaccurate predictions of the EPMA measurements in this study indicates that it is our understanding of the process at the very shallow analysis depths and low energies explored in this investigation that is somewhat lacking. One potential area of error is the effect of the layer interfaces on the electron scattering. Monte Carlo modelling considers interactions within bulk materials but even the high-fidelity PENELOPE algorithms treat layer interfaces as simply a change in medium. Any trajectories that cross an interface are treated as two distinct segments joined at the interface (Salvat, 2015). Even the sharpest interfaces are likely to be atomically perfect, but the effect this might have would be difficult to quantify and the magnitude of the effect difficult to predict.

5 Summary and Conclusions

Highly reactive metals such as U can grow several nm of oxide effectively instantaneously on contact with air and, without recourse to inert atmosphere sample

preparation and transfer systems, cannot be analysed oxide-free. At 5 kV the surface oxide can cause a 30% error in quantification of the substrate.

Neither SE imaging nor measurement of the Duane-Hunt limit identified any surface charging on the UO_2 reference material used to calibrate the U $M\alpha$ measurements. However, comparisons of analyses using the RM uncoated and carbon coated showed significant differences, with the uncoated results producing unacceptably high U k-ratios. Thus, surface charging does not appear explain the poor behaviour of the uncoated material. Unfortunately, at this point, no alternative mechanism can be proposed. Carbon coating the RM required correction for the reduced U intensity, with the magnitude of correction increasing with decreasing accelerating voltage: At 5 kV the correction increased to ~30%. The coating thickness was measured at approximately 11 nm using the C $K\alpha$ intensity, considerably less than the 15 nm indicated by the colour change of a polished brass witness block co-located with the RM in the coater. Correcting for an 11 nm C-coating, in combination with correction for the sample surface oxide, reduced the error at 5 kV to 6% but correcting for a 15 nm coating reduced this to better than 2%. As discussed above in the section on Reference Material Coating, at low accelerating voltages substrate quantification becomes very sensitive to the RM coating thickness. The optical (brass witness block colour-change) method appears to give a more reliable measure of the carbon coating thickness but the 'true' C thickness probably lies somewhere between 11 and 15 nm.

Measurement of the C $K\alpha$ peak identified interference from the U N_6-O_4 line. Utilising the higher resolution of the second order C $K\alpha$ peak position on an LDE2 diffracting element reduced the overlap correction to 1% on UC at 10 kV, and this was fully compensated for using an overlap correction.

After correction for U on C interference and for the thickness of the RM coating and sample surface oxide the U metal substrate composition could be recovered to within ±1% accuracy down to 7 kV and -1.7% at 5 kV and are indicated to increase rapidly below this. From this we can conclude that, with suitable corrections, U analyses can be carried out down to ~7 kV but are not reliable below this.

The analysis totals as a function of accelerating voltage show a consistent trend, indicating a remaining systematic error. Deviation of the oxide stoichiometry from the assumed UO_2 has too small an influence to account for this error. Measurement of the O $K\alpha$ and U $M\alpha$ absorbed by U MAC values as 9528 cm^2/g and 798 cm^2/g respectively using the P&P method (Pouchou & Pichoir, 1990) showed good agreement with a recent study (Pöml & Llovet, 2020) and with the default values in GMRFilm. Comparison of quantifications using the default GMRFilm MACs and a combination of the P&P method measured values and the recent FFAST database values showed a decreasing difference as the absorption path lengths in the sample decreased with decreasing accelerating voltage, from 0.5% at 25 kV to approximately zero at 5 kV and so also do not account for the residual error.

Both GMRFilm and PENEPMA in combination with modelling of the surface layers can significantly reduce but not completely remove analysis errors. That both programs produce such similar results implies that it is the accuracy of our understanding of the electron-sample interactions at low voltages that is the limiting factor rather than the relative fidelity or method of calculation of the models.

Whilst this investigation focusses on uranium many of the issues are also applicable both to other radioactive (RA) metals, such as Pu, and to non-RA high Z metals and alloys. These results on this highly simplistic system also provide a firm basis for extending the study to binary and then more complex alloys.

40

Credit authorship contributing statement

M.B. Matthews: Conceptualization, Methodology, Investigation, Formal analysis, Writing – original draft. **S.J. Kearns:** Writing – review and editing. **B. Buse:** Writing – review and editing.

Declaration of competing interest

The authors have no affiliation with any organization with a direct or indirect financial interest in the subject matter discussed in the manuscript.

Acknowledgements

Abbreviations

EPMA	electron probe microanalyser / microanalysis
FEG	field emission gun
FWHM	full width at half maximum
LDE	layered diffracting element
MAC	mass attenuation coefficient
RA	radioactive
RM	reference material

References

ALLEN, G. C., CROFTS, J. A. & GRIFFITHS, A. J. (1976). Infrared Spectroscopy of the Uranium/Oxygen System. *Journal of Nuclear Materials* **62**, 273–281.

BASTIN, G. F. & HEIJLIGERS, H. J. M. (1991). Nonconductive Specimens in the Electron Probe Microanalyzer - A Hitherto Poorly Discussed Problem. In *Electron Probe Quantitation*, Heinrich, K. F. J. & Newbury, D. E. (Eds.), pp. 163–175. New York: Plenum Press.

———— (1992). Quantitative EPMA of the Ultra-Light Elements Boron Through Oxygen. In *Electron Microbeam Analysis: Mikrochimica Acta Supplement*, Boekestein, A. & Pavicevic, M. K. (Eds.), pp. 19–36. Vienna: Springer.

BEARDEN, J. A. (1967). X-Ray Wavelengths and X-Ray Atomic Energy Levels. *Reviews of Modern Physics* **39**, 78–124.

BEARDEN, J. A. & BURR, A. F. (1967). Reevaluation of X-ray atomic energy levels. *Reviews of Modern Physics* **39**, 125–142.

BERA, S., SALI, S. K., SAMPATH, S., NARASIMHAN, S. V. & VENUGOPAL, V. (1998). Oxidation state of uranium: An XPS study of alkali and alkaline earth uranates. *Journal of Nuclear Materials* **255**, 26–33.

BOWLES, J. F. W. (1978). Quantitative Microprobe Analysis of Uranium Minerals. *The Microscope* **26**, 55–67.

BUSE, B., KEARNS, S. L., CLAPHAM, C. & HAWLEY, D. (2016). Decontamination in the Electron Probe Microanalysis with a Peltier-Cooled Cold Finger. *Microscopy and Microanalysis* **22**, 981–986.

BUSKER, G. (2002). 'Solution and Migration of Impurity Ions in UO2, U3O8 and Y2O3'.

Imperial College London http://abulafia.mt.ic.ac.uk/publications/theses/busker/.

CHERNIA, Z., BEN-ELIYAHU, Y., KIMMEL, G., BRAUN, G. & SARIEL, J. (2006). The Initial Stage of Uranium Oxidation : Mechanism of UO 2 Scale Formation in the Presence of a Native Lateral Stress Field. *Journal of Physical Chemistry B* **110**, 23041–23051.

COLBY, J. W. (1963). *Electron Microprobe Examination of Uranium*. Cincinnati.

———— (1966). The Applicability of Theoretically Calculated Intensity Corrections in Microprobe Analysis. In *The Electron Microprobe*, McKinley, T., Heinrich, K. F. J. & Wittry, D. B. (Eds.), pp. 95–188. New York: John Wiley and Sons, Inc.

DROUIN, D., COUTURE, A. R., JOLY, D., TASTET, X., AIMEZ, V. & GAUVIN, R. (2007). CASINO V2.42 - A fast and easy-to-use modeling tool for scanning electron microscopy and microanalysis users. *Scanning* **29**, 92–101.

DUANE, W. & HUNT, F. L. (1915). On X-Ray Wave-Lengths. *Physical Review* **6**, 166–172. http://link.aps.org/doi/10.1103/PhysRev.6.166.

FARTHING, I. R. & WALKER, C. T. (1990). *Heinrichs Mass Absorption Coefficients (For the K, L and M X-Ray Lines). Technical Note: K0290140. Commission of the European Communities, Joint Research Centre*. Karlsruhe.

HAKKILA, E. A., WATERBURY, G. R. & METZ, C. F. (1964). *Electron Microprobe Examination of Delta-Stabilized Plutonium. Los Alamos Report LA-3125*.

HEINRICH, K. F. J. (1986). Mass Absorption Coefficients for Electron Probe Microanalysis. In *11th International Congress on X-ray Optics and Microanalysis*, Brown, J. D. & Packwood, R. H. (Eds.), pp. 67–119. London, Canada: University Western Ontario.

HENKE, B. L., GULLIKSON, E. M. & DAVIS, J. C. (1993). X-ray Interactions: Photoabsorption,

Scattering, Transmission, and Reflection at E = 50-30,000 eV, Z = 1-92. *Atomic Data and Nuclear Data Tables* **54**, 181–342.

HENKE, B. L., LEE, P., TANAKA, T. J., SHIMABUKURO, R. L. & FUJIKAWA, B. K. (1982). Low-energy X-ray Interaction Coefficients: Photoabsorption, Scatering and Reflection. *Atomic Data and Nuclear Data Tables* **27**, 1–144.

HOLLEY, C. (1965). *Thermodynamics and transport properties of uranium dioxide and related phases*. Vienna
http://www.iaea.org/inis/collection/NCLCollectionStore/_Public/24/071/24071477.pdf
.

JEFFERY, B. M. (1967). Microanalysis of inclusions in irradiated UO2. *Journal of Nuclear Materials* **22**, 33–40.

JOY, D. C. & LUO, S. (1989). An Empirical Stopping Power Relationship for Low-Energy Electrons. *Scanning* **11**, 176–180.

KERRICK, D. M., EMINHIZER, L. B. & VILLAUME, J. F. (1973). The Role of Carbon Film Thickness in Electron Microprobe Analysis. *American Mineralogist* **58**, 920–925.

KITAMURA, K., SAKANE, K. & SHUNSAKU, K. (1982). X-Ray Microanalysis of Uranium on Fibrous Amidoxime-type Adsorbent. *Bulletin of the Chemical Society of Japan* **55**, 2305–2306. papers2://publication/uuid/9DCDEC89-324A-4A42-B898-2167A41B8A8D.

KLEYKAMP, H. (1981). Wavelengths of the M X-Ray Spectra of Uranium, Neptunium, Plutonium, and Americium. *Zeitschrift fur Naturforschung A* **36**, 1388–1390.

LLOVET, X. & SALVAT, F. (2016). PENEPMA: a Monte Carlo programme for the simulation of X-ray emission in EPMA. *IOP Conference Series: Materials Science and Engineering* **109**,

012009. http://stacks.iop.org/1757-

899X/109/i=1/a=012009?key=crossref.a51935eedff3118ec3e813133d747cf3.

Love, G., Cox, M. G. C. & Scott, V. D. (1974). Electron probe microanalysis using oxygen x-

rays : II . Absorption correction models. *J. Phys. D: Appl. Phys.* **7**, 2142–2155.

Matthews, M. B. (2016). Performance Characteristics of WDS and EDS Detectors. In *12th*

EMAS Regional Workshop on Electron Probe Microanalysis of Materials Today, 8 - 11

May 2016, Podor, R. (Ed.), pp. 83–114. Bagnols-sur-Ceze: EMAS and CEA Marcoule.

Matthews, M. B., Buse, B. & Kearns, S. L. (2019). Electron Probe Microanalysis Through

Coated Oxidized Surfaces. *Microscopy and Microanalysis* **25**, 1112–1129.

Matthews, M. B., Kearns, S. L. & Buse, B. (2018a). The Accuracy of Al and Cu Film Thickness

Determinations and the Implications for Electron Probe Microanalysis. *Microscopy and*

Microanalysis **24**, 83–92.

———— (2018b). Electron Beam-Induced Carbon Erosion and the Impact on Electron Probe

Microanalysis. *Microscopy and Microanalysis* **24**, 612–622.

McEachern, R. J. & Taylor, P. (1998). A review of the oxidation of uranium dioxide at

temperatures below 400°C. *Journal of Nuclear Materials* **254**, 87–121.

McSwiggen, P. (2014). Characterisation of sub-micrometre features with the FE-EPMA. *IOP*

Conference Series: Materials Science and Engineering **55**, 1–12.

McSwiggen, P., Mori, N., Takakura, M. & Nielsen, C. (2011). Improving Analytical Spatial

Resolution with the JEOL Field Emission Electron Microprobe. *Microscopy and*

Microanalysis **17**, 624–625.

http://www.journals.cambridge.org/abstract_S1431927611003990.

MERLET, C. (1998). Quantification Procedures in EPMA. In *Electron Probe Microanalysis Today. Practical Aspects. Proceedings 3rd Regional Workshop EMAS*, Llovet, X., Merlet, C. & Salvat, F. (Eds.), pp. 176–191. Barcelona: Universitat de Barcelona.

PINARD, P. T. (2016). 'Electron probe microanalysis of carbon containing steels at a high spatial resolution'. RWTH Aachen University http://publications.rwth-aachen.de/record/673259/files/673259.pdf.

PÖML, P. & LLOVET, X. (2020). Determination of Mass Attenuation Coefficients of Th, U, Np, and Pu for Oxygen Kα X-Rays Using an Electron Microprobe. *Microscopy and Microanalysis* **26**, 194–203.

POUCHOU, J.-L. & PICHOIR, F. (1988). Determination of Mass Absorption Coefficients for Soft X-Rays by Use of the Electron Microprobe. In *Microbeam Analysis 1988: Proceedings of the 23rd Annual Conference of the Microbeam Analysis Society, Milwaukee, Wisconsin, 8-12 August 1988*, Newbury, D. E. (Ed.), pp. 319–324. San Francisco: San Francisco Press.

———— (1990). Surface Film X-Ray Microanalysis. *Scanning* **12**, 212–224.

RANZETTA, G. V. T. & SCOTT, V. D. (1964). Electron-probe micoanalysis of low atomic number elements. *British Journal of Applied Physics* **15**, 263–274.

REED, S. J. B. (1975). *Electron Microprobe Analysis*. Cambridge: Cambridge University Press.

RITCHIE, N. W. M. (2009). Spectrum simulation in DTSA-II. *Microscopy and Microanalysis* **15**, 454–468.

ROMIG JR., A. D. (1984). Quantitative X-ray microanalysis of uranium alloys with the analytical electron microscope. *Journal of Microscopy* **135**, 191–202.

RUSTE, J. & GANTOIS, M. (1975). A Quantitative Analysis of Very Light Elements by the Electron Probe Microanalyser. *Journal of Physics D: Applied Physics* **8**, 872–890.

SALOMAN, E. B., HUBBELL, J. H. & SCOFIELD, J. H. (1988). X-ray Attenuation Cross Sections for Energies 100 eV to 100 keV and Elements Z = 1 to Z = 92. *Atomic Data and Nuclear Data Tables* **38**, 1–196.

SALVAT, F. (2015). PENELOPE-2014. A Code System for Monte Carlo Simulation of Electron and Photon Transport. http://www.oecd-nea.org/lists/penelope.html.

SCOTT, V. D. (1961). Electron beam micro-analysis of some plutonium-iron alloys. *Journal of Nuclear Materials* **2**, 284–293. http://linkinghub.elsevier.com/retrieve/pii/0022311561901969%5Cnhttp://www.scien cedirect.com/science/article/pii/0022311561901969.

SCOTT, V. D. & RANZETTA, G. V. T. (1961). Quantitative Analysis of the Plutonium-Iron System. *Journal of the Institute of Metals* **90**, 160–167.

SENANAYAKE, S. D., ROUSSEAU, R., COLEGRAVE, D. & IDRISS, H. (2005). The reaction of water on polycrystalline UO2: Pathways to surface and bulk oxidation. *Journal of Nuclear Materials* **342**, 179–187.

SKOMURSKI, F. N., WANG, J. W., EWING, R. C. & BECKER, U. (2013). Charge distribution and oxygen diffusion in hyperstoichiometric uranium dioxide UO2+x(x ≤ 0.25). *Journal of Nuclear Materials* **434**, 422–433. http://dx.doi.org/10.1016/j.jnucmat.2011.09.003.

WALDO, R. A. (1988). An Iteration Procedure to Calculate Film Compositions and Thicknesses in Electron-Probe Microanalysis. In *Microbeam Analysis*, Newbury, D. E. (Ed.), pp. 310–314. San Francisco: San Francisco Press.

WALKER, C. T. (1999). Assessment of the radial extent and completion of recrystallisation in high burn-up UO2 nuclear fuel by EPMA. *Journal of Nuclear Materials* **275**, 56–62.

YOUNES, C. M., ALLEN, G. C. & EMBONG, Z. (2007). Auger Electron Spectroscopic Study of the Surface Oxidation of Uranium-Niobium Alloy {U-6 wt.% Nb} in a UHV Environment Containing Primarily H2, H2O and CO. *Surface Science* **601**, 3207–3214.